Effect of Oxygen Gas Inclusion in Ar Carrier Gas in Si/SiO$_x$ Nanomaterial Synthesis using Tandem Modulated Induction Thermal Plasmas

Rio Okano[1], Y. Nagase[1], Y. Tanaka[1], Y. Nakano[1], T. Ishijima[1], S. Sueyasu[2], S. Watanabe[2], K. Nakamura[2]

[1]*Faculty of Electrical & Computer Eng., Kanazawa Univ., Kanazawa, Japan*
[2]*Research Center for Production & Technol., Nisshin Seifun Group Inc., Fujimino, Japan*

Abstract: The influence of O_2 introduction in Ar carrier gas was studied on silicon and silicon oxide (Si/SiO$_x$) nanomaterial synthesis using tandem pulse-modulated induction thermal plasmas (Tandem-PMITP) with time-controlled feeding of feedstock (TCFF) method by numerical simulation and experimental approach. The numerical simulation showed the higher temperature cooling rate in the reaction chamber for O_2 inclusion. In addition, the effects of O_2 in Tandem-PMITP were experimentally investigated on the morphology and crystal composition of the produced materials.

Keywords: Thermal plasma, Modulation, Si/SiO$_x$ nanomaterials

1. Introduction

Recently, the demand for rechargeable batteries is increasing with the spread of electric vehicles (EV) and various electronic devices. Lithium ion batteries (LIBs) are currently the most widely used rechargeable batteries. Current LIBs use graphite as the anode material with charge-discharge capacity of 0.37 Ah/g. However, this charge-discharge capacity of graphite anode is insufficient for the future large-capacity demand. The Si nanomaterial is one promising candidate for anode material in the next-generation LIB [1]. This is because Si has a theoretical charge-discharge capacity of 4.7 Ah/g, about 10 times higher than graphite [2]. It has further been reported that nanoparticulation of Si avoids electrode cracking in lithiation /delithiation to improve its cycle life. Nowadays, various type of all-solid state batteries (ASSB) have been developed for the next generation secondary batteries. Among them, there have also been reported for ASSB with nano-particulated Si anodes [3]. On the other hand, SiO nanomaterials have also attracted attention as another approach to improve cycle life [4]. SiO has the advantage of high theoretical capacitance of 2.60 Ah/g and a lower coefficient of volume expansion of 2.0, which suppresses electrode cracking to provide high cycle characteristics. It has been reported that the nanomaterialization of SiO further improves the cycle characteristics [5].

We have been developing the mass production method for nanomaterials including nanoparticles and nanowires [6, 7]. Our original method uses pulse-modulated induction thermal plasma (PMITP) with time-controlled feeding of feedstock (TCFF). The PMITP is sustained by the coil current modulated into a rectangular waveform, providing time-varying thermofluid field. The TCFF offers the feedstock powder feeding which is time-controlled to the PMITP. This PMITP+TCFF method can efficiently provide large amounts of nanoparticles [6]. Furthermore, we have developed a Tandem-PMITP which has two RF coils in one plasma torch. This Tandem-PMITP has both robustness against disturbance and larger modulation in the temperature fields which is necessary for mass production of nanoparticles [7].

In this paper, the effect of O_2 introduction in Ar carrier gas was investigated on the thermofluid field in Tandem-PMITP for nanomaterial synthesis by numerical simulation first. After that, experiment was conducted for Si/SiO$_x$ nanomaterials using Tandem-PMITP + TCFF method with O_2 introduction. Results show that Si/SiO$_x$ nanoparticles and nanowires were found to be synthesized.

2. Numerical simulation of Tandem-PMITP fields with O_2 in carrier gas

2.1. Torch and chamber configuration for calculation

In order to study the influence of O_2 inclusion in Ar carrier gas in Tandem-PMITP, numerical simulation was carried out. Fig .1(a) shows the Tandem-PMITP torch and the reaction chamber used in this model. The Tandem-PMITP torch contains two coaxial quartz tubes and two 8-turn RF coils. The quartz tube is 440 mm long and has an inner diameter of 70 mm. The inner quartz tube wall is cooled by flowing water to keep the wall temperature 300 K. The two 8-turn RF coils were installed around the quartz tube in series. These two 8-turn RF coils have supplied RF electric currents with different operation frequencies from different RF power supplies to generate electromagnetic fields inside the torch. Argon sheath gas is introduced from the top of the torch along the inner wall of the torch with swirl flow. Along the center axis of the torch, a 150 mm-long metallic water-cooled tube was inserted from the top of the torch. Through this metallic tube, the feedstock powder was supplied directly into the thermal plasma with a carrier gas in the experiments. Downstream of the torch, the reaction chamber is installed. Fig .1(b) depicts the calculation space in the numerical simulation. This space corresponds to the cross section of the Tandem-PMITP torch and the reaction chamber. The space was divided into 114 axial and 65 radial divisions for numerical simulation.

2.2. Calculation conditions

Table 1 summarizes the fixed common conditions. The time-averaged input power was set to 10 kW from each

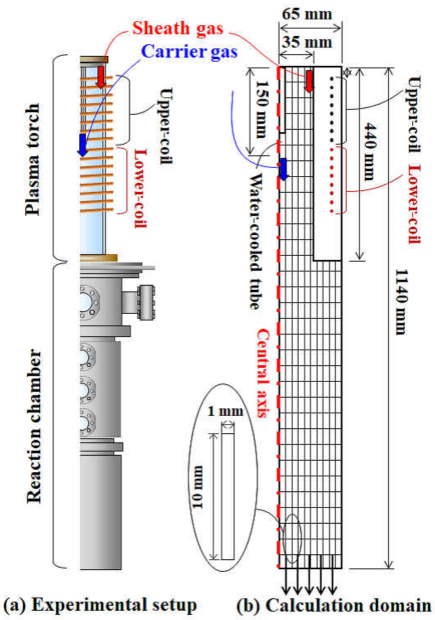

Fig. 1. Schematic of Tandem-PMITP system (a) and the corresponding calculation domain (b).

coil irrespective of coil current modulation. The upper coil current was not modulated, while the lower coil current was amplitude-modulated in a rectangular waveform. The shimmer current level (SCL), which was defined as a ratio of lower current level to higher current level, for the lower coil current modulation was 50%. The modulation cycle was set to 20 ms. The duty factor (DF), which indicates the ratio of on-time to one modulation cycle, was set to 50%. The sheath gas Ar was 90 slpm. The total flow rate of the carrier gas was fixed at 4 slpm. Table 2 shows the comparison condition. Under the above fixed common condition, O_2 flow rate in the carrier gas was set at 0 and 1.0 slpm to study the influence of O_2 inclusion on the time-varying temperature field in Tandem-PMITP. The feedstock was not supplied.

In the numerical simulation, the mass, momentum, and energy conservation equations were solved considering electromagnetic fields from the upper and the lower coil currents by SIMPLE method. The O_2 transport equation was also simultaneously solved to obtain the O_2 content distribution.

2.3. Time variation in temperature distribution

Fig. 2 shows the gas temperature T_g distribution (left panel) and the O_2 mass fraction distribution (right panel) at a time t=10 ms with and without O_2 introduced at 1.0 slpm, respectively. The time t=10 ms corresponds to the timing with highest input power from the lower coil. As seen, injection of carrier gas cools the thermal plasma on the axis around axial position of $150 < z < 210$ mm in Fig. 2(a), because of the cooling effect by cold Ar carrier gas injection. In addition, O_2 inclusion further decreases the temperature on the axis as shown in Fig. 2(b). This further decreases in temperature originates from the power consumption of O_2 dissociation in case of O_2 inclusion. On the other hand, in the reaction chamber below the torch, the temperature was found to be decreased inward in the radial direction by cold entrainment gas flow irrespective of O_2 inclusion or not. This entrainment gas flow is induced by the modulation operation of the Tandem-PMITP. The Tandem-PMITP causes the time-varying temperature, which involves the mass density change and then the gas flow field in the power modulation. As seen in Fig. 2(b), this entrainment gas flow was stronger in case of O_2 introduction, showing the temperature drops to around 2000 K around (r, z)=(20 mm, 650 mm). This temperature drop by this strong entrainment gas flow may cool the Si+O+SiO vapor more efficiently and convert it into nuclei for nanoparticle formation. Furthermore, O_2 inclusion in carrier gas offers wide O_2 distribution in the lower coil region in the torch and in the reaction chamber as depicted in Fig. 2(b).

Table 1. Common calculation conditions with/without O_2 gas inclusion.

Fixed parameters	Value
Time-averaged input power	Upper : 10 kW
	Lower : 10 kW
Upper-coil frequency	420 kHz
Lower-coil frequency	210 kHz
Number of coil turn	Upper : 8 turn
	Lower : 8 turn
Modulation(On/Off time)	Upper : 100%DF-100%SCL
	Lower : 50%DF-50%SCL
Modulation cycle	20 ms
Sheath gas flow rate	Ar: 90 slpm (L/min)
Pressure	300 torr

Table 2. Comparison conditions with/without O_2 gas inclusion.

Variable parameters	Value	
$Ar+O_2$	4+0 slpm	3+1 slpm

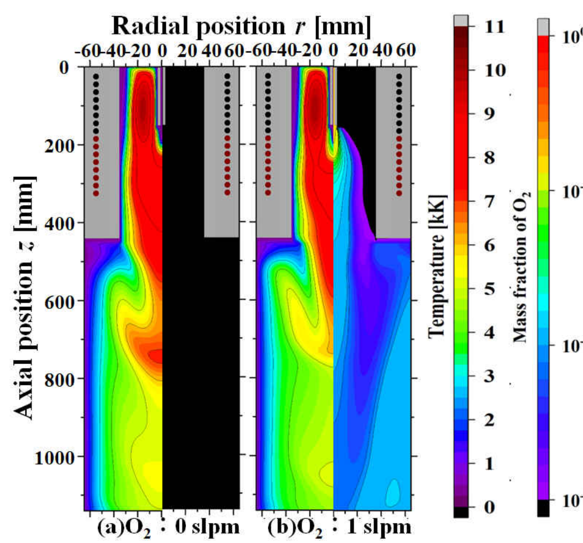

Fig. 2. Gas temperature distribution and mass fraction distribution of O_2 with/without O_2 gas inclusion at t=10 ms in Tandem-PMITP.

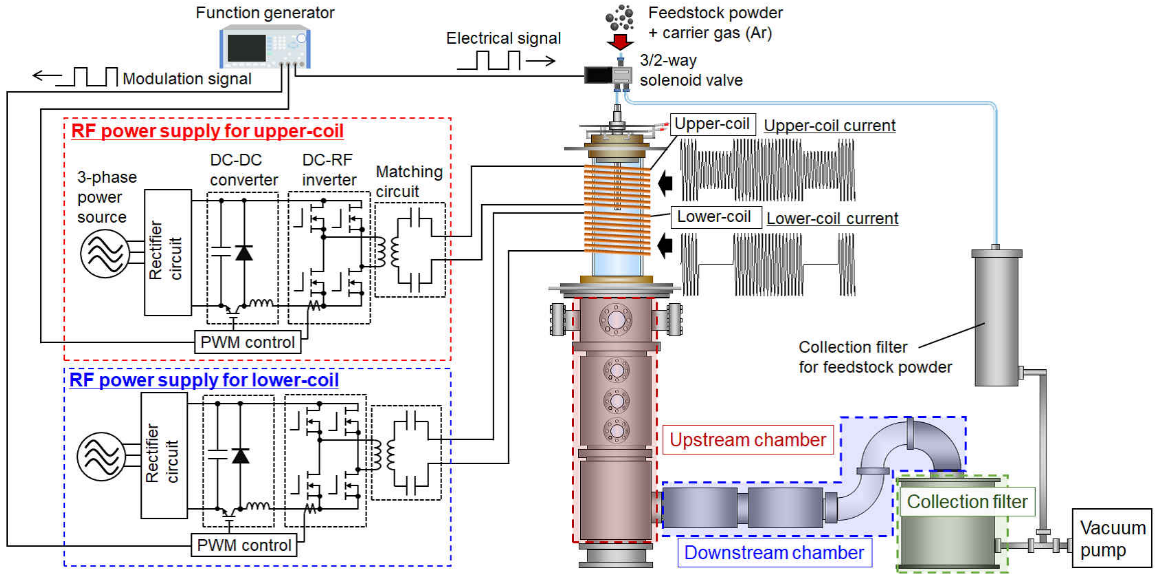

Fig. 3. Experimental setup for nanomaterial synthesis by Tandem-PMITP + TCFF method.

3. Si/SiO$_x$ nanomaterial synthesis experiments

3.1. Experimental setup

The experiment for Si/SiO$_x$ nanomaterials was conducted using Tandem-PMITP + TCFF method. Fig. 3 demonstrates the experimental setup for nanomaterial synthesis using Tandem- PMITP. This experimental setup has one plasma torch almost similar configuration to that in the numerical simulation. Each of the upper and lower coils was connected with each of individual two RF power supplies operated at different operating frequencies of 410 kHz and 245 kHz. The adoption of different frequencies for the upper and the lower coils is to avoid the influence of electromagnetic coupling between the upper and lower coil circuits and RF power sources. The Tandem-PMITP is sustained by these upper and lower coil currents in one plasma torch. Downstream of the plasma torch installed the reaction chamber including the upstream chamber and the downstream chamber and the collection filter with a vacuum pump. The synthesized nanomaterials were collected mainly in the collection filter.

3.2. Experimental conditions

This experimental condition is almost similar to the calculation condition in the previous section except some ones. The modulation condition of the lower coil current was set to 66%DF and 20%SCL, while the upper coil current was not modulated. Table 3 indicates the variable condition. The oxygen flow rate in the carrier gas was set to 0 and 0.5 slpm. The feedstock was Si powder with a mean diameter of 26 μm. This feedstock Si powder was introduced with the carrier gas intermittently at valve opening cycle of 40%DF$_{\text{valve}}$, synchronously with the On-time of the lower coil current. This synchronized feeding of feedstock to Tandem-PMITP promotes the feedstock evaporation.

Table 3. Experimental condition.

Variable parameters	Value	
Condition	(i)	(ii)
Ar+O_2	4+0 slpm	3.5+0.5 slpm
Feed rate	6.13 g/min	5.13 g/min

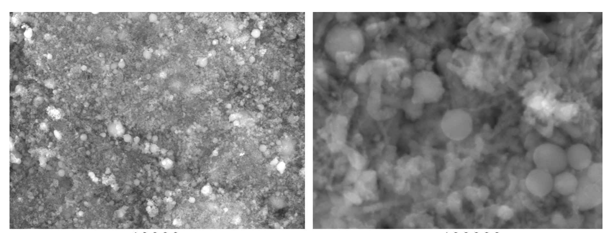

(a) O_2 : 0 slpm

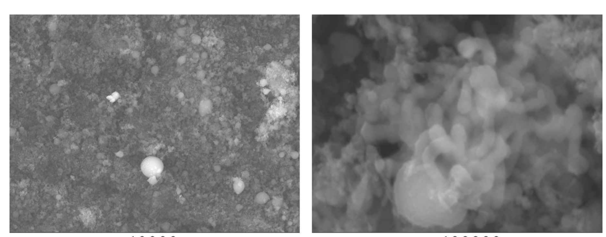

(b) O_2 : 0.5 slpm

Fig. 4. FE-SEM images of synthesized Si/SiO$_x$ nanomaterials with/without O_2 gas inclusion; (a) O_2 of 0 slpm, (b) O_2 of 0.5 slpm.

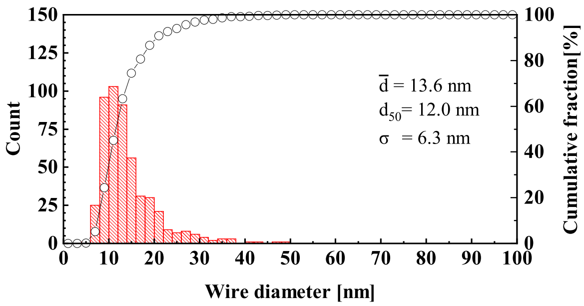

(a) O_2 : 0 slpm

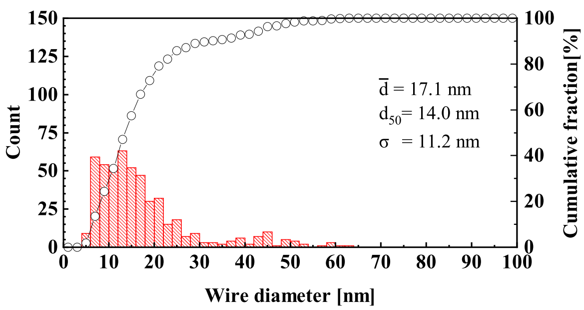

(b) O_2 : 0.5 slpm

Fig. 5. Diameter distribution of synthesized nanowires with/without O_2 gas inclusion; (a) O_2 of 0 slpm, (b) O_2 of 0.5 slpm.

3.3. Experimental results

Fig. 4 shows the FE-SEM images of the nanomaterials synthesized under the conditions of O_2 flow rates of 0 and 0.5 slpm. From Fig. 4(a) for no O_2 inclusion, the synthesized nanomaterials were a mixture of nanoparticles and a small amount of nanowires. On the other hand, it is seen from Fig. 4(b) that O_2 inclusion of 0.5 slpm made the synthesized material more nanowire-like. In other words, O_2 inclusion promotes to produce nanowires. From the FE-SEM image, 500 nanowires were randomly selected, and the diameter frequency distribution was estimated by measuring the diameter of the nanowires. Fig. 5 shows the estimated diameter frequency distribution for each condition. For little O_2 inclusion, the mean diameter of nanowires are 13.6 nm. The mean nanowire diameter increased with O_2 introduction of 0.5 slpm. For O_2 inclusion of 0.5 slpm, the mean diameter is 17.1 nm, which indicates that O_2 inclusion produces thicker nanowires with more fraction of nanowires to nanoparticles.

For the synthesized nanomaterials, XRD analysis was conducted. Fig. 6 shows the XRD analysis results for the synthesized nanomaterials. In these figures, strong crystalline peaks of Si(1 1 1), Si(2 2 0) and Si (3 1 1) were detected, indicating polycrystalline Si nanomaterials were formed. Furthermore, a broad peak derived from amorphous Si/SiO_x were observed in both conditions. The broad peaks became stronger as the flow rate of O_2 was increased. This showed that amorphous nanosized SiO_x were synthesized. From the above results, Si/SiO_x nanomaterials were found to be generated by introducing O_2 in the carrier gas.

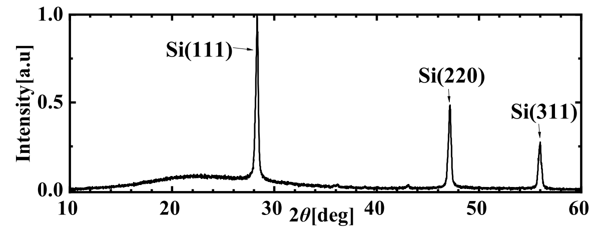

(a) O_2 : 0 slpm

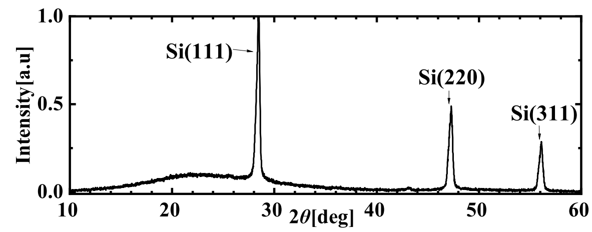

(b) O_2 : 0.5 slpm

Fig. 6. XRD of synthesized nanomaterials with/without O_2 gas inclusion; (a) O_2 of 0 slpm, (b) O_2 of 0.5 slpm.

4. Conclusion

In this paper, the effect of O_2 introduction in Ar carrier gas was investigated on the thermofluid field in Tandem-PMITP for nanomaterial synthesis. Introduction of O_2 was found to decrease temperature in the reaction chamber and then to create stronger entrainment gas flow, showing more cooling the vapor. Experiment was conducted for Si/SiO_x nanomaterials using Tandem-PMITP + TCFF method with O_2 introduction. Results show that Si/SiO_x nanomaterials were found to be produced.

References

[1] X. Su, et al., Adv. Energy Mater., **6**, 7393 (2015)

[2] A. Mukhhopadhyay, et al., Prog. Mater. Sci., **63**, 58 (2014).

[3] N. Ohta, et al., ACS Appl. Energy Mater., **2**, 7005 (2019)

[4] J. H. Yom, et al., J. Power Sources, **311**, 159 (2016)

[5] R. Miyazaki, et al., J. Power Sources, **329**, 41 (2016)

[6] N. Kodama, et al., J. Phys. D: Appl. Phys., **49**, 305501 (2016)

[7] R. Furukawa, et al., Plasma Chem. & Plasma Process., **42**, 435 (2022)